

Mpemba effect in a Langevin system: population statistics, metastability and other exact results

Apurba Biswas,^{1,2, a)} R. Rajesh,^{1,2, b)} and Arnab Pal^{1,2, c)}

¹⁾*The Institute of Mathematical Sciences, C.I.T. Campus, Taramani, Chennai 600113, India*

²⁾*Homi Bhabha National Institute, Training School Complex, Anushakti Nagar, Mumbai 400094, India*

The Mpemba effect is a fingerprint of the anomalous relaxation phenomenon wherein an initially hotter system equilibrates faster than an initially colder system when both are quenched to the same low temperature. Experiments on a single colloidal particle trapped in a carefully shaped double well potential have demonstrated this effect recently [*Nature* **584**, 64 (2020)]. In a similar vein, here, we consider a piece-wise linear double well potential that allows us to demonstrate the Mpemba effect using an exact analysis based on the spectral decomposition of the corresponding Fokker-Planck equation. We elucidate the role of the metastable states in the energy landscape as well as the initial population statistics of the particles in showcasing the Mpemba effect. Crucially, our findings indicate that neither the metastability nor the asymmetry in the potential is a necessary or a sufficient condition for the Mpemba effect to be observed.

I. INTRODUCTION

The Mpemba effect refers to the faster equilibration of a hotter system compared to a colder system when both are quenched to a final temperature which is the lowest¹. Initially studied in water^{1–9}, the effect has now been established as a more general anomalous relaxation phenomenon. There now exists a wide range of physical systems where experimental evidences about the existence of the Mpemba effect have been reported. Examples include magnetic alloys¹⁰, polylactides¹¹, clathrate hydrates¹², and colloidal systems^{13–15}.

There has been a great deal of theoretical effort to demonstrate the Mpemba effect in spin systems^{16–21}, spin glasses²², molecular gases in contact with a thermal reservoir^{23–26}, Markovian systems with restricted phase space^{27,28}, Langevin systems^{29–33}, active systems³⁴, quantum systems^{35–37}, systems with phase transitions^{19,38–40}, and granular systems^{41–48}. Spanning across various physical systems, different causes have been attributed to the Mpemba effect although no unified consensus exists to the underlying reason. However, it turns out that in the analytically tractable kinetic state models or in the Langevin systems, the so-called “multi-dimensional rugged energy landscape” picture provides an effective description of the Mpemba effect. In particular, the presence of one or multiple metastable minima in the free energy can trap a system at a lower energy more effectively than the same at higher temperature, resulting in a faster relaxation of the hotter system.

More on the experimental side, the Mpemba effect was demonstrated by Kumar and Bechhoefer in a system of a colloidal particle diffusing in a confining double well quartic potential with linear slopes near the do-

main boundaries¹³. It was shown that the asymmetry in the potential, which was realized by introducing different widths for the left- and the right- end domains, is a key factor for the Mpemba effect. As the asymmetry in the domain widths is being increased, even a stronger version of the Mpemba effect emerges where the relaxation is exponentially faster for a hotter system. Notwithstanding demonstrating this remarkable anomalous relaxation phenomena, there are a few yet fundamental frontiers that still remain open. For example, can asymmetry in the potential depths (in addition to the asymmetric domains) result in the Mpemba effect? Is there a necessary or a sufficient ‘asymmetry’ condition on the nature/shape of the potential that can universally underpin the Mpemba effect? Another question that intrigues our mind along this line: Is a double well potential necessary to realize the Mpemba effect in Langevin systems? A recent study showed the Mpemba effect in a simple piece-wise constant potential configuration where the minima of the potentials were set at neutral equilibrium²⁹ thus breaking down our general intuitions based on the rugged landscape, metastability and dis-balanced statistics of the particles’ population.

In this paper, we delve deeper into these questions by investigating an exactly solvable model. Similar to the experiment by Kumar and Bechhoefer¹³, we consider a system of an overdamped Brownian particle trapped in a double well potential. However, the potential is constructed in a piece-wise linear manner which makes the problem solvable. The major advantage besides its analytical tractability is that one can also gain deep insights from this canonical model by scanning several potential configurations. For example, in our set-up, the potential can be made asymmetric in several different ways: (a) different widths for the left and right domains of the potential as discussed in the experiment by Kumar and Bechhoefer¹³, (b) same domain widths but asymmetric location of the potential minima, (c) different depths of the potential wells, and (d) different heights for the left, center and right edge of the potential (see

^{a)}Electronic mail: apurbab@imsc.res.in

^{b)}Electronic mail: rrajesh@imsc.res.in

^{c)}Electronic mail: arnabpal@imsc.res.in

Fig. 1). The potential can also be transformed into a single well by taking certain limits. Solving for the time evolution of the probability distribution function using the method of eigenspectrum decomposition of the corresponding Fokker-Planck equation^{49,50}, we present a comprehensive analysis of the relaxation phenomena in terms of the eigenvalues and the distant functions for each of the above-mentioned cases. Our extensive analysis underpins the following observations: (i) asymmetry of domain widths is not a necessary condition for the existence of the Mpemba effect, (ii) asymmetry in the potential heights is not a sufficient condition for the Mpemba effect, and (iii) presence of the metastable states is neither a necessary nor a sufficient condition for this anomalous relaxation.

The remainder of the paper is organized as follows. We describe our model system in Sec. II. For this set-up, we sketch out the eigenspectrum decomposition method for solving the probability distribution function with suitable matching and boundary conditions. In Sec. III, we introduce the distance functions which measures the deviation of a transient state from an equilibrium state. Sec. IV discusses the role of population statistics of the Brownian particle across the double well potential landscape. We pinpoint the role of metastable states and discuss the variation in the population statistics of the Brownian particle as a result of the potential modulation. In Sec. V, we explore several ‘typical’ and ‘atypical’ configurations of the double well potential and illustrate the existence of the Mpemba effect. We provide two complete phase diagrams that demonstrate the possible configurations of the potential difference and hot-to-final temperature ratio where the Mpemba effect can be observed. Various intriguing facts are highlighted. In Sec. VI, we demonstrate the existence of the Mpemba effect in the absence of metastable states and discuss the intricate interplay between the population statistics and the initial kinetic energy of the Brownian particle that leads this effect. We conclude our paper in Section VII with a brief summary and discussion.

II. MODEL AND GENERAL FORMALISM

We consider a colloidal particle diffusing in an asymmetric double well potential $\tilde{U}(x)$, as shown in Fig. 1, in a thermal environment characterized by noise η and damping γ . The mean and variance of the noise are

$$\langle \eta(t) \rangle = 0 \quad \text{and} \quad \langle \eta(t)\eta(t') \rangle = 2\gamma k_B T_b \delta(t-t'), \quad (1)$$

where T_b is the temperature of the thermal bath and k_B is the Boltzmann’s constant. We consider the overdamped case where the damping γ is large compared to the mass of the particle. Motion of the particle is then described by the overdamped Langevin equation

$$\gamma \frac{dx}{dt} = -\frac{d\tilde{U}}{dx} + \eta(t). \quad (2)$$

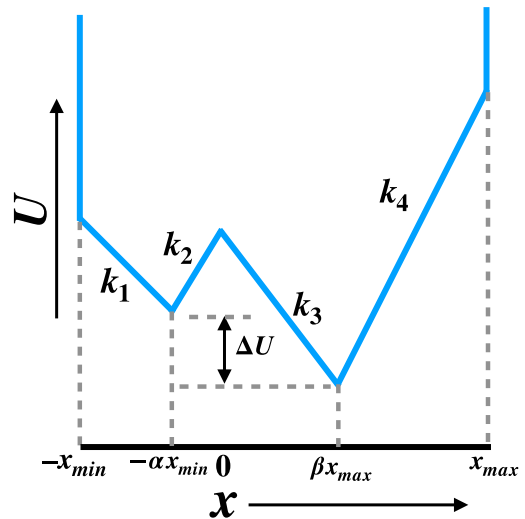


FIG. 1. Schematic diagram of the piece-wise linear double well potential. The boundaries of the potential are situated at $-x_{min}$ and x_{max} . The two minima of the double well potential are located at $-\alpha x_{min}$ and βx_{max} , where $\alpha, \beta \in (0, 1)$. The parameters k_1, k_2, k_3 and k_4 refer to the various slopes. ΔU depicts the difference between the depths of the two wells.

The corresponding Fokker-Planck equation for the probability distribution function $p(x, t)$ reads^{49,51}

$$\frac{\partial p}{\partial t} = \frac{\partial}{\partial x} \left[\frac{1}{\gamma} \frac{d\tilde{U}}{dx} p \right] + D \frac{\partial^2 p}{\partial x^2}, \quad (3)$$

where D is the diffusion coefficient and is related to the temperature via the Einstein’s relation⁴⁹

$$D = \frac{k_B T_b}{\gamma}. \quad (4)$$

In here, we will solve $p(x, t)$ analytically for the given configuration of the potential. To this end, it will be first useful to review the formalism of eigenspectrum decomposition for solving the Fokker-Planck equation (3) in the presence of a generic confining potential.

A. Spectral decomposition

To layout the formalism we closely follow Risken⁴⁹. We start by normalizing the potential in terms of $k_B T_b$ so that

$$U(x) = \frac{\tilde{U}(x)}{k_B T_b}. \quad (5)$$

Thus, Eq. (3) simplifies to the continuity equation

$$\frac{\partial p}{\partial t} = D \frac{\partial}{\partial x} \left[\frac{dU}{dx} p \right] + D \frac{\partial^2 p}{\partial x^2} = -\frac{\partial J}{\partial x}, \quad (6)$$

from where the probability current/flux can be identified as

$$J(x) = -D \left[\frac{dU}{dx} + \frac{\partial}{\partial x} \right] p = -D e^{-U(x)} \frac{d}{dx} \left[e^{U(x)} p \right], \quad (7)$$

and the corresponding Fokker-Planck operator reads

$$\mathcal{L}_{FP} = D \frac{\partial}{\partial x} \left(\frac{dU}{dx} \right) + D \frac{\partial^2}{\partial x^2}. \quad (8)$$

The stationary solution of the Fokker-Planck Eq. (6) for the probability density is given by the Boltzmann distribution at temperature T_b

$$\pi(x, T_b) = \frac{e^{-U(x)}}{\mathcal{Z}}, \quad (9)$$

where $\mathcal{Z} = \int e^{-U(x)} dx$ is the partition function. Note that the Fokker-Planck operator in Eq. (8) is not self-adjoint. A simple transformation leads to its self-adjoint form \mathcal{L} where

$$\mathcal{L} = e^{U(x)} \mathcal{L}_{FP} e^{-U(x)} = D \frac{\partial^2}{\partial x^2} - V(x), \quad (10)$$

and

$$V(x) = \frac{D}{4} \left(\frac{dU}{dx} \right)^2 - \frac{D}{2} \frac{d^2 U}{dx^2}, \quad (11)$$

is now the effective potential. Thus the original problem is now reduced to analyzing the following eigenvalue problem

$$\mathcal{L} \psi_n = \lambda_n \psi_n, \quad (12)$$

where ψ_n are the eigenfunctions of the self-adjoint Fokker-Planck operator \mathcal{L} corresponding to the eigenvalue λ_n . Denoting the eigenvectors of the Fokker-Planck operator \mathcal{L}_{FP} as $\phi_n(x)$ and noting that both of them have the same eigenvalues, one can write⁴⁹

$$\psi_n(x) = e^{\frac{U(x)}{2}} \phi_n(x). \quad (13)$$

The eigenvalues λ_n follow the order: $\lambda_1 = 0 > \lambda_2 > \lambda_3 \dots$, where $\lambda_1 = 0$ corresponds to the stationary distribution for a bath temperature, T_b . The first eigenvector corresponding to $\lambda_1 = 0$ is given by $\psi_1(x) = e^{-U(x)/2} / \sqrt{\mathcal{Z}(T_b)}$.

Given the initial probability condition $p(x', 0)$, the probability distribution function $p(x, t)$ can be obtained as

$$p(x, t) = \int W(x, t|x', 0) p(x', 0) dx', \quad (14)$$

where the transition probability or the propagator $W(x, t|x', 0)$ of the Fokker-Planck equation can be written in terms of the eigenfunctions and eigenvalues (see^{49,51})

$$\begin{aligned} W(x, t|x', 0) &= e^{\mathcal{L}_{FP} t} \delta(x - x') \\ &= e^{-\frac{U(x)}{2} + \frac{U(x')}{2}} \sum_n e^{\lambda_n t} \psi_n(x) \psi_n^*(x'). \end{aligned} \quad (15)$$

Substituting the transition probability into Eq. (14), one finds

$$p(x, t) = \int dx' e^{-\frac{U(x)}{2} + \frac{U(x')}{2}} \sum_n e^{\lambda_n t} \psi_n(x) \psi_n^*(x') p(x', 0). \quad (16)$$

Since $\lambda_1 = 0$, we can rewrite Eq. (16) as follows

$$p(x, t) = \frac{e^{-U(x)}}{\mathcal{Z}(T_b)} + \sum_{n \geq 2} a_n e^{-\frac{U(x)}{2}} \psi_n(x) e^{-|\lambda_n| t}, \quad (17)$$

where

$$a_n = \int dx' p(x', 0) e^{\frac{U(x')}{2}} \psi_n^*(x'). \quad (18)$$

At large times, since $\lambda_2 > \lambda_3$, to leading order, we obtain

$$p(x, t) \simeq \frac{e^{-U(x)}}{\mathcal{Z}(T_b)} + a_2 e^{-\frac{U(x)}{2}} \psi_2(x) e^{-|\lambda_2| t}, \quad t \gg \frac{1}{|\lambda_3|}. \quad (19)$$

The equation above is central to further analysis of the relaxation properties for the particle in the potential $\tilde{U}(x)$.

B. Shape of the potential

The form of the potential well is crucial to the observation of the Mpemba effect as was demonstrated in the experiment¹³. In there, $\tilde{U}(x)$ is considered to be a double well quartic potential with linear slopes near its boundaries or domain walls. Furthermore, the potential is confined in an asymmetric domain and it was shown that the asymmetry in the widths of the left and right domains about the origin can lead to the Mpemba effect¹³.

Likewise, we consider a double well potential which is piece-wise linear. In contrast to the quartic double well potential, this problem is exactly solvable as will be evident below. The boundaries of the well are situated at $(-x_{min}, x_{max})$. For simplicity, we set $k_B T_b = 1$. The potential in Fig. 1 can be quantified in the following way

$$U(x) = \begin{cases} -k_1 x, & -x_{min} < x < -\alpha x_{min} \\ k_2 x + \alpha(k_1 + k_2)x_{min}, & -\alpha x_{min} < x < 0 \\ -k_3 x + \alpha(k_1 + k_2)x_{min}, & 0 < x < \beta x_{max} \\ k_4 x + [\alpha(k_1 + k_2) - \beta(k_3 + k_4)]x_{max}, & \beta x_{max} < x < x_{max}, \end{cases} \quad (20)$$

where k_1 , k_2 , k_3 and k_4 are slope constants that play a crucial role in designating the potential various shapes and the two constants $\alpha, \beta \in (0, 1)$.

The asymmetry in the shape of the potential can be introduced through various parameters such as different domain widths about the origin, different positions of the two wells about the origin or due to the different depths of the potential wells. However, it turns out that the different heights of the two wells is a key factor to the observation of the Mpemba effect in contrary to the result shown in Ref.¹³. This potential set-up provides an amenable physical interpretation for underlying cause in such systems as will be discussed and illustrated in Sec. IV.

C. Jump conditions

The potential in Eq. (20) is not differentiable at $x = -\alpha x_{min}$, 0 and βx_{max} , and diverges at the boundaries $x = -x_{min}$ and $x = x_{max}$. Let x_- and x_+ denote the points just to the left and right of boundary of a linear segment. For the choice of potential $U(x_+) = U(x_-)$ while $U'(x_+) \neq U'(x_-)$. Across a boundary, both the probability currents are equal, i.e., $J(x_+, t) = J(x_-, t)$, as well as the probabilities are equal. Thus, from Eq. (7), we obtain

$$-U'(x_+)p(x_+, t) - \frac{\partial p(x_+, t)}{\partial x} = -U'(x_-)p(x_-, t) - \frac{\partial p(x_-, t)}{\partial x}. \quad (21)$$

$$p(x_+, t) = p(x_-, t). \quad (22)$$

The jump conditions in Eqs. (21) and (22) are satisfied by each of the eigenfunctions, and hence from Eq. (16), we have

$$\begin{aligned} \psi'_n(x_+) + \frac{U'(x_+)\psi_n(x_+)}{2} &= \psi'_n(x_-) + \frac{U'(x_-)\psi_n(x_-)}{2} \\ \psi_n(x_+) &= \psi_n(x_-). \end{aligned} \quad (23)$$

At the boundaries, the potential diverges. This implies that the probability current must vanish and it leads to the following condition in terms of the eigenfunctions

$$\psi'_n(x) + \frac{U'(x)}{2}\psi_n(x) = 0, \text{ at } x = -x_{min}, x_{max}. \quad (25)$$

The jump conditions [Eqs. (24), (23) and (25)] are utilized to solve the eigenspectrum of the Fokker-Planck operator \mathcal{L} [see Eq. (12)] as discussed in the next section.

D. Eigenspectrum analysis

We have the task to solve the following eigenvalue problem

$$\mathcal{L}\psi_n = -|\lambda_n|\psi_n, \quad (26)$$

where ψ_n are the eigenfunctions of the self-adjoint Fokker-Planck operator \mathcal{L} [see Eq. (10)] corresponding to the eigenvalue λ_n . We solve this equation separately in each of the four domains of the potential $U(x)$, characterized by slopes k_1 , k_2 , k_3 , and k_4 . This will lead to eight constants of integration which will be determined by the jump conditions at the boundaries of the regions, leading to a transcendental equation for the eigenvalue. Each of these cases is discussed in below.

1. Region I: $-x_{min} < x < -\alpha x_{min}$

In this given region, we have $U'(x) = -k_1$. Then, Eq. (26) takes the form:

$$\frac{d^2\psi_n^I}{dx^2} + \left(\frac{\lambda_n}{D} - \frac{k_1^2}{4}\right)\psi_n^I = 0, \quad (27)$$

which has the solution

$$\psi_n^I(x) = A_n \sin(m_{1n}x) + B_n \cos(m_{1n}x), \quad (28)$$

where A_n, B_n are constants and

$$m_{1n} = \sqrt{\frac{\lambda_n}{D} - \frac{k_1^2}{4}}. \quad (29)$$

The solutions for the eigenfunctions in the other regimes are similar, but with different constants. We list them below.

2. Region II: $-\alpha x_{min} < x < 0$

Here, we have $U'(x) = k_2$ and the solution for the eigenfunction is

$$\psi_n^{II}(x) = C_n \sin(m_{2n}x) + D_n \cos(m_{2n}x), \quad (30)$$

where

$$m_{2n} = \sqrt{\frac{\lambda_n}{D} - \frac{k_2^2}{4}}. \quad (31)$$

3. Region III: $0 < x < \beta x_{max}$

In this case, we have $U'(x) = -k_3$ and the solution reads

$$\psi_n^{III}(x) = E_n \sin(m_{3n}x) + F_n \cos(m_{3n}x), \quad (32)$$

where

$$m_{3n} = \sqrt{\frac{\lambda_n}{D} - \frac{k_3^2}{4}}. \quad (33)$$

4. Region IV: $\beta x_{max} < x < x_{max}$

In here, we have $U'(x) = k_4$ and the solution for the eigenfunction is given by

$$\psi_n^{IV}(x) = G_n \sin(m_{4n}x) + H_n \cos(m_{4n}x), \quad (34)$$

where

$$m_{4n} = \sqrt{\frac{\lambda_n}{D} - \frac{k_4^2}{4}}. \quad (35)$$

E. Boundary and matching conditions

We now determine the different constants using the matching and boundary conditions. While the boundary conditions [see Eq. (25)] are associated with the divergence of the potential at the boundaries leading to the vanishing probability current, the matching conditions [see Eqs. (23) and (24)] arise at the boundaries of the potential domains due to the continuity of the probability current.

1. Boundary condition at $x = x_{max}$:

The infinite jump in potential at $x = x_{max}$ leads to the vanishing probability current. It is given by the boundary condition [Eq. (25)] which in terms of the eigenfunction ψ_n^{IV} reads

$$\psi_n^{IV'}(x_{max}) + \frac{U_4'(x_{max})}{2} \psi_n^{IV}(x_{max}) = 0. \quad (36)$$

$$\begin{aligned} & C_n \left[m_2 \cos(m_2 \alpha x_{min}) - \frac{k_2}{2} \sin(m_2 \alpha x_{min}) \right] + D_n \left[m_2 \sin(m_2 \alpha x_{min}) + \frac{k_2}{2} \cos(m_2 \alpha x_{min}) \right] \\ &= B_n \left[(m_1 \nu_{1n} - \frac{k_1}{2}) \cos(m_1 \alpha x_{min}) + (m_1 + \frac{\nu_{1n} k_1}{2}) \sin(m_1 \alpha x_{min}) \right], \end{aligned} \quad (44)$$

and

$$-C_n \sin(m_2 \alpha x_{min}) + D_n \cos(m_2 \alpha x_{min}) = B_n [\cos(m_1 \alpha x_{min}) - \nu_{1n} \sin(m_1 \alpha x_{min})], \quad (45)$$

respectively. The coefficients C_n and D_n are solved using

Substituting for ψ_n^{IV} from Eq. (34), we obtain

$$\begin{aligned} G_n &= -\nu_{4n} H_n, \\ \nu_{4n} &= \frac{\frac{k_4}{2} \cos(m_{4n} x_{max}) - m_{4n} \sin(m_{4n} x_{max})}{\frac{k_4}{2} \sin(m_{4n} x_{max}) + m_{4n} \cos(m_{4n} x_{max})}. \end{aligned} \quad (37)$$

Thus,

$$\psi_n^{IV}(x) = H_n [\cos(m_{4n}x) - \nu_{4n} \sin(m_{4n}x)]. \quad (39)$$

2. Boundary condition at $x = -x_{min}$:

Similar to the boundary condition at $x = x_{max}$, there is a divergence in the potential at $x = -x_{min}$ in the form of an infinite jump. The boundary condition in Eq. (25), in terms of the eigenfunctions ψ_n^I , is then given by

$$\psi_n^{I'}(-x_{min}) + \frac{U_1'(-x_{min})}{2} \psi_n^I(-x_{min}) = 0. \quad (40)$$

Substituting for ψ_n^I from Eq. (28), we obtain

$$A_n = \nu_{1n} B_n, \quad (41)$$

$$\nu_{1n} = \frac{\frac{k_1}{2} \cos(m_{1n} x_{min}) - m_{1n} \sin(m_{1n} x_{min})}{\frac{k_1}{2} \sin(m_{1n} x_{min}) + m_{1n} \cos(m_{1n} x_{min})}. \quad (42)$$

Thus,

$$\psi_n^I(x) = B_n [\cos(m_{4n}x) + \nu_{1n} \sin(m_{4n}x)]. \quad (43)$$

We now use the jump conditions associated with the continuity of the probability current [see Eqs. (23) and (24)] across the boundaries of the potential domains at $x = -\alpha x_{min}$, 0 and $x = \beta x_{max}$. They are given by the following three matching conditions.

3. Matching condition at $x = -\alpha x_{min}$

At $x = -\alpha x_{min}$, the eigenfunctions $\psi_n^I(x)$ and $\psi_n^{II}(x)$ satisfy the matching conditions given by Eqs. (23) and (24) which simplifies to

Eqs. (45) and (44) in terms of B_n and the expressions are

given in Eqs. (A1) and (A2) of Appendix A.

4. Matching condition at $x = 0$

Similar to the above, the eigenfunctions $\psi_n^{II}(x)$ and $\psi_n^{III}(x)$ satisfy the matching conditions given by Eqs. (23) and (24) for the continuity of the probability current at $x = 0$ which simplifies to

$$E_n = \frac{m_2}{m_3} C_n + \frac{k_2 + k_3}{2m_3} D_n, \quad (46)$$

$$F_n = D_n. \quad (47)$$

5. Matching condition at $x = \beta x_{max}$:

At $x = \beta x_{max}$, the matching conditions given by Eqs. (23) and (24) is satisfied by the eigenfunctions $\psi_n^{III}(x)$ and $\psi_n^{IV}(x)$, which simplifies to

$$\begin{aligned} & C_n \frac{m_2}{m_3} \sin(m_3 \beta x_{max}) \\ & + D_n \left(\frac{k_2 + k_3}{2m_3} \sin(m_3 \beta x_{max}) + \cos(m_3 \beta x_{max}) \right) \\ & = H_n \left[\cos(m_4 \beta x_{max}) - \nu_{4n} \sin(m_4 \beta x_{max}) \right], \end{aligned} \quad (48)$$

and

$$\begin{aligned} & C_n \left[m_2 \cos(m_3 \beta x_{max}) - \frac{k_3}{2} \frac{m_2}{m_3} \sin(m_3 \beta x_{max}) \right] \\ & + D_n \left[\frac{k_2}{2} \cos(m_3 \beta x_{max}) \right. \\ & \left. - \left(m_3 + \frac{k_3(k_2 + k_3)}{4m_3} \right) \sin(m_3 \beta x_{max}) \right] \\ & = H_n \left[\left(\frac{k_4}{2} - \nu_{4n} m_4 \right) \cos(m_4 \beta x_{max}) \right. \\ & \left. - \left(\frac{\nu_{4n} k_4}{2} + m_4 \right) \sin(m_4 \beta x_{max}) \right], \end{aligned} \quad (49)$$

respectively. The coefficients C_n and D_n are solved in terms of H_n using Eqs. (48) and (49) and the expressions are given in Eqs. (A3) and (A4) of Appendix A. Now, we consider the ratios of Eqs. (A1), (A2), (A3) and (A4) that form a transcendental equation to solve for the eigenvalues λ_n . Thus, solving for the eigenvalues λ_n in turn helps to find the constants A_n , B_n , C_n , D_n , E_n , F_n and H_n .

III. DISTANCE FUNCTION AND THE MPEMBA EFFECT

How to quantify the Mpemba effect as an anomalous relaxation phenomena? To see this, let us consider two systems: first one P , initially equilibrated at temperature T_h and second one Q , initially equilibrated at temperature T_c where $T_h > T_c$. These initial equilibrium distributions are denoted by $\pi(T_h)$ and $\pi(T_c)$ respectively.

Now imagine that both P and Q are quenched at once to a common bath temperature, T_b , where $T_h > T_c > T_b$. Eventually, both of them will equilibrate to the common distribution $\pi(T_b)$ given long enough time. The Mpemba effect is said to exist if P equilibrates faster than Q during the transient/relaxation process.

To quantify this relaxation process, let us now define the *distance from equilibrium function*, $D[p(t), \pi(T_b)]$ which measures the instantaneous distance of a distribution $p(x, t)$ from the final equilibrium Boltzmann distribution, $\pi(T_b)$. It has been argued (see²⁷ and others) that the Mpemba effect is independent of $D[p(t), \pi(T_b)]$ provided that the distance measure obeys the following properties: (a) If $T_h > T_c > T_b$, then the distance from equilibrium function should follow the order $D[\pi(T_h), \pi(T_b)] > D[\pi(T_c), \pi(T_b)]$, (b) $D[p(t), \pi(T_b)]$ should be a monotonically non-increasing function of time, and (c) $D[p(t), \pi(T_b)]$ should be a convex function of $p(x, t)$.

Notably, there are many well-adapted measures that exist in the literature namely the entropic distance, L_1 or norm distance and the Kullback-Leibler (KL) divergence^{13,27,30}. Thus, as a working definition, if one has $D[\pi(T_h), \pi(T_b)] > D[\pi(T_c), \pi(T_b)]$ initially for $T_h > T_c$ followed by $D[p^h(t), \pi(T_b)] < D[p^c(t), \pi(T_b)]$ at a later time, we will state that the Mpemba effect exists.

In the rest of the article, we will use the “ L_1 or norm” measure for the distance from equilibrium function. More precisely, this is defined as

$$D[p(t), \pi(T_b)] \equiv L_1(t) = \int dx |p(x, t) - \pi(x, T_b)|. \quad (50)$$

Now substituting the form of $p(x, t)$ from Eq. (19) into the above equation, we find

$$D[p(t), \pi(T_b)] = \sum_{n \geq 2} |a_n e^{-\frac{U(x)}{2}} \psi_n(x)| e^{-|\lambda_n|t}. \quad (51)$$

The condition for the Mpemba effect, as mentioned above, now boils down to

$$|a_2(T_c)| \equiv |a_2^c| > |a_2^h| \equiv |a_2(T_h)|. \quad (52)$$

The condition demands that $|a_2(T)|$ should have a non-monotonic behavior with the increase in temperature. Note that the coefficient a_2 is calculated using Eq. (18) and is a function only of the initial temperature and the bath temperature. Also, $a_2(T)$ is zero at the final temperature $T = T_b$ since the eigenvectors are orthonormal.

IV. MODULATION OF THE POTENTIAL AND POPULATION – CONNECTION TO THE EXPERIMENTS

Following the colloidal experiment by Kumar and Bechhoefer, we learnt that the asymmetry in the shape of the double well potential plays an important role to the Mpemba effect. In particular, it was shown that there is no such effect if the asymmetry in the width of the left

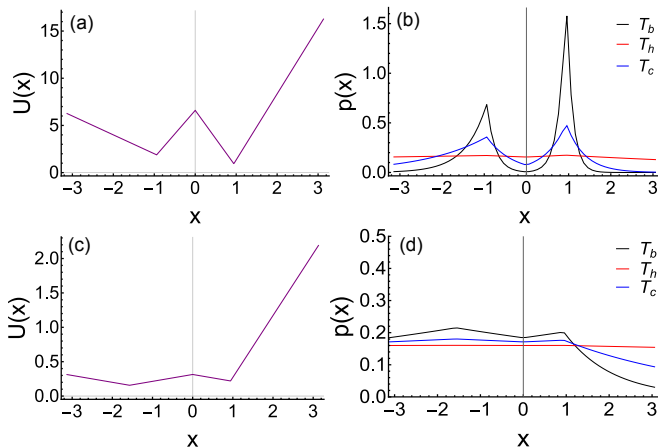


FIG. 2. Modulation of the potential and its effect on the population distribution of the Brownian particle in the two wells. Panel (a) and (c) corresponds to different configurations of the potential well. The parameters of the potential in (a) are chosen to be $\alpha = 0.3$, $\beta = 0.3$, $x_{min} = \pi$, $x_{max} = \pi$, $D = 1$, $k_1 = 2$, $k_2 = 5$, $k_3 = 6$ and $k_4 = 7$ and in (c) $\alpha = 0.5$, $\beta = 0.3$, $|x_{min}| = \pi$, $x_{max} = \pi$, $D = 1$, $k_1 = 0.1$, $k_2 = 0.1$, $k_3 = 0.1$ and $k_4 = 0.9$. Panels (b) and (d) depict the population distribution corresponding to the external potentials in (a) and (c) respectively for the initial temperatures T_h (red), T_c (blue) and final temperature T_b (black) with $T_h > T_c > T_b$.

and right domains of the potential vanishes¹³. In this section, we aim to revisit these limits from our model system by suitably changing the potential barrier.

To this end, let us turn our attention to Figs. 2(a) and 2(c) which show two different configurations for the potential barrier. The modulation of the potential barrier leads to a rearrangement in the population of the Brownian particle between the two wells for the two different temperatures as shown in Fig. 2(b) and 2(d).

In Fig. 2(a), we consider a configuration of a potential with a considerable potential barrier between the two minima. The corresponding population distribution of the Brownian particle for the temperatures T_h , T_c and T_b , i.e., for the hot, cold and the bath temperatures respectively is shown in Fig. 2(b). The initially colder system is more populated in the lowest well compared to the initially hotter system. However, there is also a considerable amount of population distributed in the metastable state for the colder system, which is not the case for the initially hotter system whose population distribution is nearly uniform i.e., it can not really ‘see’ the metastable state. As a result, post quenching, the population distribution of the colder system takes a significant amount of time to rearrange and eventually relax to the lowest energy well from the metastable state. On the other hand, the initially hotter system ends with a higher population in the lowest well due to its fast relaxation. This feature grants an advantage to the initially hotter system over the colder one, and the Mpemba effect is observed.

Next, we consider the potential shown in Fig. 2(c), where the potential barrier between the two minima is

almost diminishing thus creating a flat barrier between the wells. In this case, the population distribution at the bath temperature, T_b which corresponds to the final equilibrium state, is almost equally populated between the two wells. Moreover, not much difference can be seen in the population distribution of the initially hot and the cold system. In other words, the ‘hindrance’ due to the metastable state in the relaxation to the equilibrium state is absent. Owing to this, the relaxation process is similar for the both initially hot and the cold system. The initially colder system (having distribution closer to the final equilibrium state) relaxes faster compared to the initially hot system and hence, no Mpemba like effect is observed.

The above physical scenarios naturally set the stage to make the connection with the experiment¹³. In particular, the asymmetry in the widths of the left and right domains of the confined potential in the experiment plays an analogous role to a finite barrier height between the wells in our model set-up. As we have shown that this configuration leads to the Mpemba effect similar to the asymmetric domain for the left and the right well of the potential in the experiment.

On the other hand, the symmetric double well potential configuration in the experiment with equal widths for the left and right domains is analogous to our second case with almost a flat barrier between the two wells of the potential [see Figs. 2(c) and (d)]. It is because the symmetric potential configuration has the population of the particle almost similarly distributed between the two wells of the potential for any temperatures eliminating the effect of the presence of any metastable state. As a result, the relaxation dynamics from an initial equilibrium distribution to the final equilibrium are similar for any temperature, and the initially cold system having an initial temperature closer to the final equilibrium state relaxes faster. Hence, no Mpemba effect can be seen. These two possible configurations thus draw physical similarities between the experiment and our system.

V. MPEMBA EFFECT IN DOUBLE WELL POTENTIAL

In this section, we showcase several key configurations of the double well potential that can lead to the Mpemba effect. These results are analyzed based on the generic criterion for the Mpemba effect as described in Sec. III. The methodology we use is as follows. Given a configuration of the potential, we solve the eigenvalue Eq. (26) to find the eigenspectrum. Once this is known, we can immediately compute the time dependent solution for the probability distribution using Eq. (17). This allows us to understand the relaxation process by looking at the slowest eigenvalue. Next, we analyze the Mpemba condition namely $|a_2^c| > |a_2^h|$ (see Sec. III). Specifically, this condition is scanned thoroughly to identify the set of initial temperatures for which $|a_2(T)|$ has a non-monotonic behavior with temperature T so that the above-mentioned

inequality is satisfied. We provide phase diagrams spanning in the parameter space of ΔU (will be discussed in the later part) and temperature ratio to underpin the desired regimes for the Mpemba effect. We make an attempt to provide physical reasoning behind all the possible cases.

It is now understood from the discussion in Sec. IV that a fully symmetric potential configuration does not lead to the Mpemba effect. In what follows, we first consider an asymmetric potential configuration. This includes equal widths for the left and right domains and equal heights at the left, center, and right edges of the potential. The only asymmetry is in the form of different depths between the two potential wells. We show in Sec. V A that the mere presence of asymmetry in the potential configuration is *not a sufficient* condition to induce the Mpemba effect. To explore further, we take other configurations that have restricted asymmetries.

This is done by keeping different heights at the left, center, and right edge of the potential. We carefully analyze these different configurations and explore the possibility of the Mpemba effect. The following configurations are of our interest: (a) equal domain widths as discussed in Sec. V B, and (b) unequal domain widths as discussed in Sec. V C. For both cases (a) and (b), we explore the different possible configurations by varying the depths of the potential wells.

A. Asymmetry is not a sufficient criterion

We start by showing that the asymmetry is not a sufficient condition for the existence of the Mpemba effect. As an example, we consider the case where the asymmetry is only in terms of different depths of the potential wells while keeping everything else symmetric, as shown in Fig. 3(a). The heights of the left, centre and right edges of the potential well are equal. Moreover, the potential minima are also situated symmetrically about the origin and at the centre of their respective domains. For this case, there is no Mpemba effect since $|a_2(T)|$ increases monotonically with T [see Fig. 3(b)]. As discussed in Sec. IV, the absence of the Mpemba effect can be explained based on the similar nature of the initial population distribution of the hot and the cold system for a particular choice of T_h and T_c respectively, as shown in the inset of Fig. 3(b), leading to similar relaxations for both the systems.

Hence, one would anticipate that additional asymmetries might be required in the potential configuration to induce the Mpemba effect. However, we find that as long as the potential heights at the left, center, and right edges are equal, there is no Mpemba effect. In what follows, further asymmetric configurations are explored by considering the cases of equal and unequal domain widths and also varying the depths between the two wells of the potential while satisfying the necessary condition that the heights at the left, center, and right edges of the po-

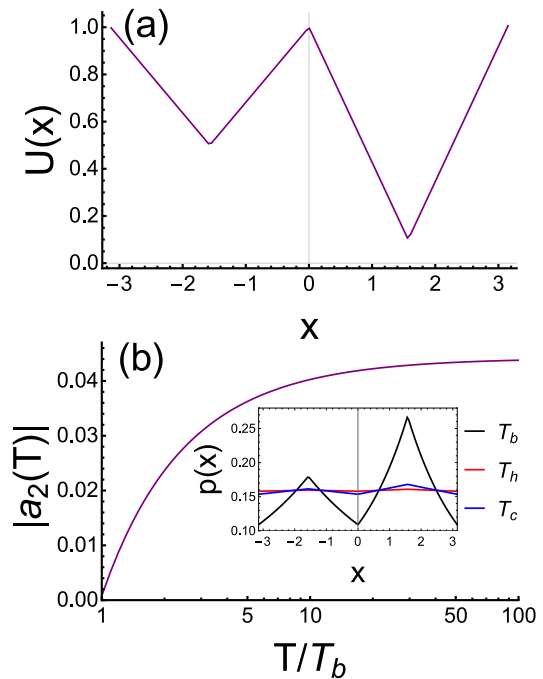


FIG. 3. Illustration of the absence of the Mpemba effect in an asymmetric double well potential indicating that *asymmetry is not sufficient*. (a) Asymmetric shape of the potential with different depths for the left and right wells while keeping all the other parameters of the potential symmetric about the origin. The potential heights at its left, center and right edges are equal and so are the positions of the two wells about the origin. The shape of the potential corresponds to the choice of the parameters $x_{max} = x_{min} = \pi$, $\alpha = \beta = 0.5$, $k_1 = k_2 = 0.32$ and $k_3 = k_4 = 0.57$. (b) Monotonic evolution of $|a_2(T)|$ with T showing the absence of the Mpemba effect. Inset: Initial population distribution of the confined Brownian particle for the chosen temperatures $T_h = 50T_b$ (red) and $T_c = 10T_b$ (blue) showing almost similarly distributed populations across the potential landscape. The final equilibrium distribution (black) corresponds to bath temperature $T_b = 1$.

tential are different.

B. Equal domain widths

We first examine the configurations of the potential with equal widths for the left and right domains. The boundaries of the well are situated at $x_{min} = x_{max}$ with the position of the two wells equidistant from the origin at $x = -\alpha x_{min}$ and $x = \beta x_{max}$ with $\alpha = \beta$. The various asymmetries in the configuration of the potential are introduced through the choice of the slopes k_1 , k_2 , k_3 and k_4 for the different domains of the confined potential. The shape of the potential with a specific choice of parameters is shown in Fig. 4(a).

The existence of the Mpemba effect for this particular configuration of the potential is evident from the non-monotonic behavior of the coefficient $|a_2(T)|$ with T as shown in Fig. 4(b). The existence of the Mpemba effect

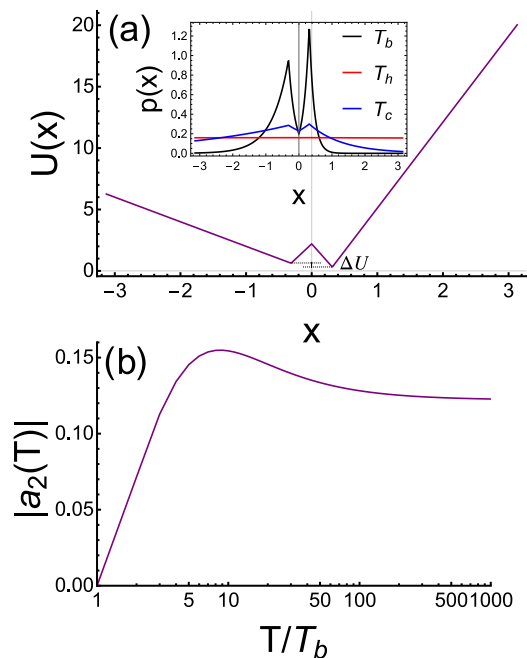


FIG. 4. Illustration of the Mpemba effect in a confined double well potential with equal domain widths. (a) Shape of the potential with equal domain widths (3 units) about the origin. The asymmetry in the potential configuration is introduced through the choice of different slopes in separate domains. The configuration of the potential is determined by the choice of the parameters: $x_{max} = x_{min} = \pi$, $\alpha = \beta = 0.1$, $k_1 = 2$, $k_2 = 5$, $k_3 = 6$ and $k_4 = 7$. Inset: Initial population distribution of the confined Brownian particle for the chosen temperatures $T_h = 1000T_b$ (red) and $T_c = 7T_b$ (blue) such that $|a_2^h| < |a_2^c|$. This shows a significant population distribution for T_c around the metastable state compared to that (which is almost flat) of T_h . The final equilibrium distribution (black) corresponds to bath temperature $T_b = 1$. (b) Non-monotonic evolution of $|a_2(T)|$ with T clearly indicates the presence of the Mpemba effect in this set-up.

for this configuration of the potential is also qualitatively evident in terms of the population distribution of the particle as shown in the inset of Fig. 4(a) for $T_h = 1000T_b$ and $T_c = 7T_b$ which satisfy the criteria for the Mpemba effect. The population distribution of the initially cold system is localised at the intermediate potential well, thus experiencing a metastable state which leads to its slower relaxation towards the final equilibrium. On the other hand, the initially hot system has uniform distribution across the potential landscape and undergoes faster relaxation to the final equilibrium distribution.

We next explore the phase space that shows the Mpemba effect, for this form of potential configuration in terms of various asymmetries. It is done by varying the depths between the two wells of the potential landscape ΔU [see Fig. 4(a)] as a function of the temperature of the initially hot system T_h while keeping the temperature of the initially cold system fixed at $T_c = 4T_b$. Changing the depths of the two wells is equivalent to making choices

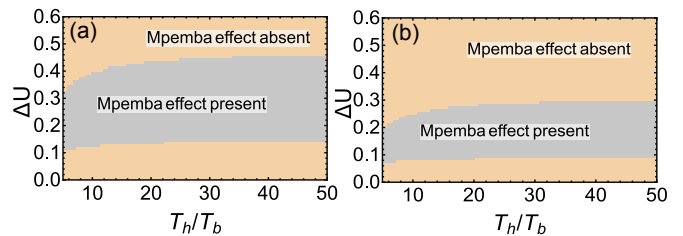


FIG. 5. ΔU - (T_h/T_b) phase diagram illustrating the region of the Mpemba effect in the case of double well potential with equal domain widths. The phase diagram is obtained by varying the depth of the right well of the potential while keeping the depth of its left well fixed and by changing the temperature ratio. The phase space is partitioned into two domains: one where the Mpemba effect is present corresponding to the criteria $|a_2^h| < |a_2^c|$, and other complementary region. The phase diagrams correspond to different choices of the position of the potential wells which are symmetric about the origin and are determined by: (a) $\alpha = \beta = 0.1$, (b) $\alpha = \beta = 0.5$.

for different possibilities of the slopes k_1 , k_2 , k_3 , and k_4 . Figures 5(a) and (b) illustrate the phase diagrams of the possible asymmetries in the potential configuration leading to the Mpemba effect, in the ΔU - (T_h/T_b) plane for two different choices of positions for the potential minima although symmetrically placed about the origin.

C. Unequal domain widths

We now consider the potential configurations with unequal domain widths and explore the phase space of various possible asymmetries that might demonstrate the Mpemba effect. This is motivated from Ref.¹³ where potential with unequal domain widths was considered in order to study the Mpemba effect.

The unequal domain widths of the potential configuration correspond to the positions of its boundaries situated at x_{min} and x_{max} respectively with the magnitudes $x_{max} \neq x_{min}$. The position of the two wells are equidistant from the origin at $x = -\alpha x_{min}$ and $x = \beta x_{max}$ with $\alpha = \beta$. For the simplicity of our analysis, the magnitude of the slopes k_1 , k_2 , k_3 , and k_4 are kept equal for different domains. Thus, the only asymmetry in the potential is introduced through the choice of different domain widths of the confined potential, and one such configuration with a particular choice of parameters is shown in Fig. 6(a).

The non-monotonic behavior of the coefficient $|a_2(T)|$ with T as shown in Fig. 6(b) illustrates the existence of the Mpemba effect for this configuration of the potential. We consider one such pair of temperatures $T_h = 50T_b$ and $T_c = 10T_b$ for the hot and cold systems respectively that satisfy the criteria $|a_2^h| > |a_2^c|$ and study the nature of the population distribution of the particle for the particular case as shown in the inset of Fig. 6(a). Here too, the cold system exhibits localisation of its population distribution in the local minima leading to slower relaxation towards the final equilibrium compared to the hot system.

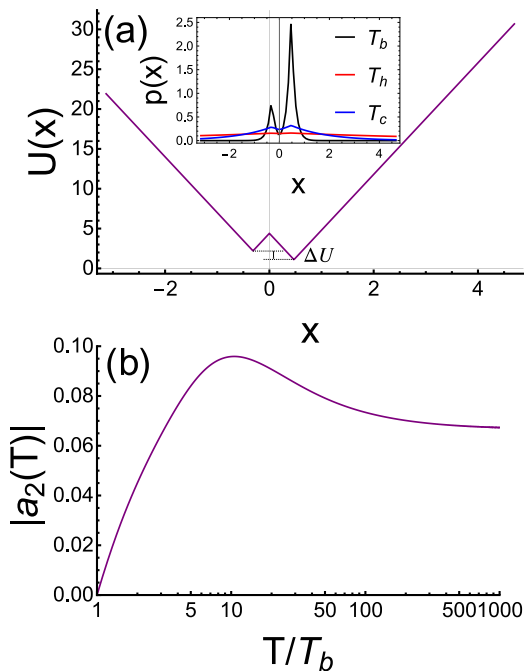


FIG. 6. Illustration of the Mpemba effect in a confined double well potential with unequal domain widths while keeping every other parameters symmetric about the origin. (a) Shape of the potential with unequal domain widths ($x_{max} \neq x_{min}$) about the origin. The position of the two wells of the potential and its various slopes are kept equal. The configuration of the potential is determined by the choice of the parameters: $x_{min} = \pi$, $x_{max} = 1.5\pi$, $\alpha = \beta = 0.1$ and $k_1 = k_2 = k_3 = k_4 = 7$. Inset: Initial population distribution of the confined Brownian particle for the chosen temperatures $T_h = 50T_b$ (red) and $T_c = 10T_b$ (blue) such that $|a_2^h| < |a_2^c|$. This shows a significant population distribution around the metastable state for T_c compared to the same for T_h . The final equilibrium distribution (black) corresponds to the bath temperature $T_b = 1$. (b) Non-monotonic evolution of $|a_2(T)|$ with T confirms the presence of the Mpemba effect in this set-up.

We now explore the phase space of possible asymmetries that leads to the Mpemba effect, for this form of potential configuration. Here, the asymmetries are introduced in terms of the choices of different slopes and different widths for the left and right domains. We explore the phase space by varying the depths between the two wells of the potential landscape ΔU [see Fig 6(a)] as a function of the temperature of the initially hot system T_h while keeping the temperature of the initially cold system fixed at $T_c = 4T_b$. Note that the variation of the two well depths is equivalent to making different choices for the slopes of the potential. We perform this exercise for two different choices of widths for the right domain respectively keeping the width of the left domain fixed as illustrated in Figs. 7 (a) and (b) respectively. As mentioned earlier, the phase diagrams allow us to provide a comprehensive picture in terms of the parameters that

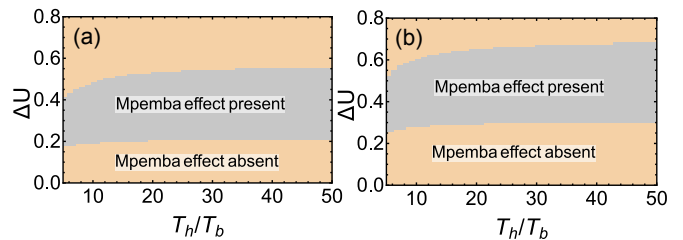


FIG. 7. ΔU -(T_h/T_b) phase diagram illustrating the region of the Mpemba effect for the case of double well potential with unequal domain widths. The phase diagram is constructed in the similar manner as in Fig. (5). The phase diagrams in the left- and right- panel correspond to different choices of the widths for the right domain of the potential: (a) $x_{max} = 1.2\pi$, (b) $x_{max} = 1.5\pi$ keeping the width of its left domain fixed at $x_{min} = \pi$. The position of the two wells are determined by the parameters $\alpha = \beta = 0.1$ for both the cases.

are pertinent to the Mpemba effect.

VI. MPEMBA EFFECT WITHOUT A METASTABLE MINIMUM

In this section, we show that the presence of metastable states is not necessary for the existence of the Mpemba effect. We demonstrate this by configuring the potential with no metastable state. In a recent study, the Mpemba effect was shown for a piece-wise constant potential where the local stability of double well potential is replaced by neutral stability²⁹. Likewise, we construct potential configurations with no metastable states and yet demonstrate the possibility of observing the Mpemba effect. In short, such an analysis would rationalize the claim that neither metastability nor neutral stability are necessary for the Mpemba effect.

Let us consider the single well potential with two linear slopes at the edges and with fixed magnitude in between $x = -\alpha x_{min}$ to $x = \beta x_{max}$ (see Fig. 8), where x_{min} and x_{max} are the boundaries where the potential goes to infinity. We find that the minimal criterion to observe the Mpemba effect in this configuration is to introduce an asymmetry in the form of different heights for the left and right edge of the potential landscape with $\alpha = \beta < 1$.

One such configuration of the potential is shown in Fig. 8(a). The existence of the Mpemba effect for this configuration is illustrated through the non-monotonic behavior of the coefficient $|a_2(T)|$ with temperature T – see Fig. 8(b). We consider one such pair of temperatures $T_h = 48T_b$ and $T_c = 6T_b$ for the initially hot and cold systems respectively that satisfy the criteria $|a_2^c| > |a_2^h|$ and study the nature of the population distribution of the Brownian particle for the particular case as shown in Fig. 8(c).

In the case of the double well potential configuration, the presence of a metastable state plays an important role in the existence of the Mpemba effect. Clearly, in

this case, there is no delay in the redistribution of the populations to the final equilibrium distribution starting from two different temperatures due to the absence of any metastable state. However, the existence of the Mpemba effect for this configuration shows that there is a trade-off between the initial population density and kinetic energy of the particle in the redistribution process to the final equilibrium as evident from the population statistics near the edge of the potential landscape [see Fig. 8(c)].

Although the initially hot system has more population of the particles near the edge of the potential to redistribute than the same of the initially cold system, the higher kinetic energy of the hot system dominates during the relaxation process for the given configuration of the potential landscape, leading to a faster relaxation of the hot system than the cold one and hence the Mpemba effect is observed.

However, keeping the same configuration of the potential landscape and same temperatures for the initial hot and the cold system, we find that the anomalous relaxation disappears as the depth of the potential minimum is decreased as is illustrated in Fig. 8(d) and (e). It is evident from the monotonically increasing nature of the coefficient $|a_2(T)|$ with temperature, T [see Fig. 8(e)] that there is no Mpemba effect in this case. The population distribution of the particle for this configuration of the potential is shown in Fig. 8(f). A qualitative argument can be given based on the trade-off between the initial population density and kinetic energy of the particles present at the edges of the potential landscape. The presence of a smaller population for the initially cold system at the edges (which would eventually redistribute to the potential minimum) dominates in the relaxation process to the final equilibrium. Naturally, one would expect that the initially cold system will approach the final equilibrium faster than the initially hot system discarding the possibility of a Mpemba effect.

Finally, we explore the phase space of the single well potential landscape with the temperature ratio. We vary the minimum or the depth of the potential landscape ΔU measured with respect to the potential height at the left edge [see Figs. 8(a) and (d)] as a function of the temperature of the initially hot system T_h while keeping the temperature of the initially cold system fixed at $T_c = 4T_b$. Figure 9 illustrates the phase diagram in the ΔU - (T_h/T_b) plane for a fixed choice of the heights for the left and right edge of the potential.

VII. CONCLUSION

In summary, we have theoretically studied the Mpemba effect in a system of an overdamped particle trapped in an external potential motivated by a similar experimental set-up¹³. The potential is generically piece-wise linear but double-welled, and moreover we can maneuver it to give various shapes. One can exactly solve this model analytically to obtain the eigenspectrum de-

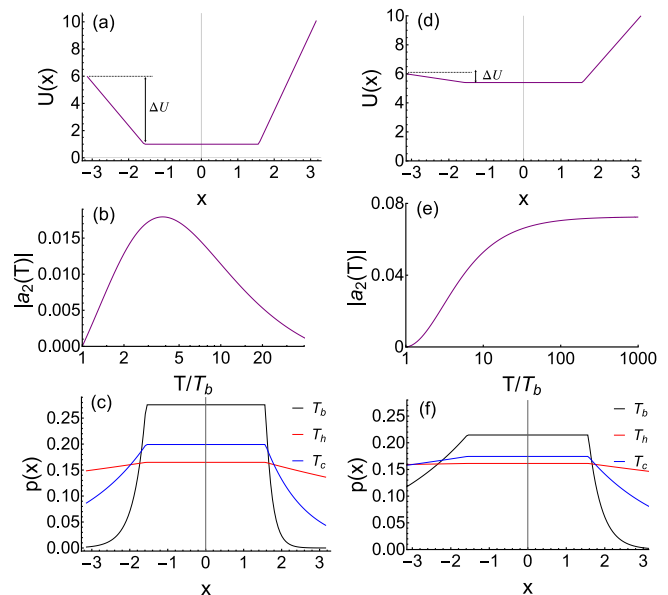


FIG. 8. Illustration of the Mpemba effect in a confined single well potential with no metastable state. (a) Shape of the single well potential is determined by the choice of the parameters: $x_{max} = x_{min} = \pi$, $\alpha = \beta = 0.5$, $k_2 = k_3 = 0$, $k_1 = 3.18$ and $k_4 = 5.73$. (b) Non-monotonic evolution of $|a_2(T)|$ with T showing the presence of the Mpemba effect. (c) Initial population distribution of the confined Brownian particle for the chosen temperatures $T_h = 48T_b$ (red) and $T_c = 6T_b$ (blue). Here, $|a_2^h| < |a_2^c|$ which shows a significant difference in the population density at the minimum of the potential well. The final equilibrium distribution (black) corresponds to bath temperature $T_b = 1$. The Mpemba effect disappears for the above configuration of the potential if the depth of the potential well is decreased as shown in (d). The modified potential configuration corresponds to a change in the slopes to $k_1 = 0.38$ and $k_4 = 2.93$ while keeping the other parameters same as in the earlier case. (e) Monotonic evolution of $|a_2(T)|$ with T shows the absence of the Mpemba effect for the modified configuration. (f) Initial population distribution of the confined Brownian particle for the same pair of temperatures $T_h = 48T_b$ (red) and $T_c = 6T_b$ (blue) show nearly similar population distribution at the minimum of the potential well.

composition of the corresponding Fokker-Planck equation. This allows us to provide a comprehensive study of the Mpemba effect spanning a wide panorama of physical scenarios.

As noted earlier in¹³ and in other works that symmetric potentials are not expected to exhibit the Mpemba effect. For symmetric potentials, a_2 is exactly zero and higher order coefficients become important. By explicit calculation, absence of the Mpemba effect was noted in piece-wise constant potential as well as the pure harmonic potential²⁹. We expect the same to hold for symmetric piece-wise linear potentials. For the class of symmetric potentials that we explored, we did not find any exceptions. Asymmetry was introduced in the experiment in Ref.¹³ through different domain widths for the two min-

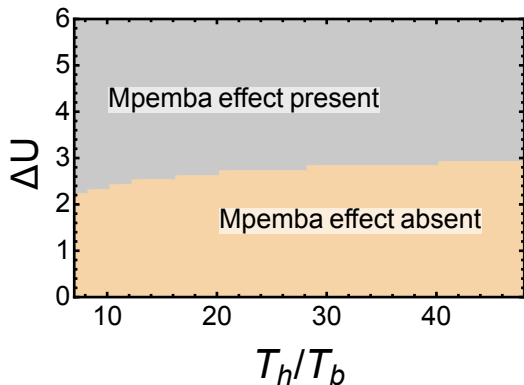


FIG. 9. ΔU - (T_h/T_b) phase diagram illustrating the region of the Mpemba effect for the case of a single well potential. The phase diagram is obtained as before by varying the depth of the potential minimum & the temperature ratio. Here, there are two distinct regions and the criterion $|a_2^h| < |a_2^c|$ marks the one where the Mpemba is observed. Here, $T_c = 4T_b$ as before and the other parameters determining the configuration of the potential are: $\alpha = \beta = 0.5$.

ima. We also demonstrate the existence of the Mpemba effect when the two widths are unequal. Through counterexamples, we also show that unequal domain widths are neither a necessary nor a sufficient condition for the Mpemba effect to be present. We also show that the Mpemba effect can be realized for equal domain widths but for other asymmetries in the potential. In particular, we find that the Mpemba effect is easily realizable when the heights of the potential at the left, center and right edges are different. This is a notable feature of our work.

Concluding, the Mpemba effect in Langevin systems is usually depicted in terms of the ruggedness in the energy landscape where the particles diffuse. The relaxation of

the colder system to the lowest energy state is usually hindered by the presence of metastable states while the hotter system does not experience (i.e., can overlook) the metastable states due to its higher energy and thus can relax to the lowest energy state faster than the colder system. In this paper, we revisit this physical picture for a variety of different cases. Generically it is understood that the larger energy barrier leads to a significant amount of population concentration at the intermediate energy well (or the metastable state) for the initially colder system as compared to the initially hotter system. This leads to the consensus that metastability might be necessary for the Mpemba effect. We benchmark this rationale within our exactly solvable model. However and in stark contrast, we also show that metastable states are not necessary for Mpemba effect by demonstrating the effect in a potential with *no metastable states*, questioning the current qualitative understanding. This result also improves on the result in Ref.²⁹, where for piece-wise constant potentials, metastability was replaced by neutral stability. Taken together these new observations, we believe that our work offers a significant aid to the current understanding of the Mpemba effect in Langevin systems. Finally, it is within our understanding that there is a subtle interplay between the initial population (manifesting the energy landscape) and the hopping frequency for particle rearrangement (which crucially depends on the temperature), however a rigorous quantification is yet to be made. This is a key aspect that requires further investigations.

VIII. ACKNOWLEDGEMENT

Arnab Pal gratefully acknowledges research support from the DST-SERB Start-up Research Grant Number SRG/2022/000080.

Appendix A: Finding the constants C_n and D_n

In this appendix, we solve for the constants C_n and D_n in terms of B_n and H_n . Solving for C_n and D_n in terms of B_n using Eqs. (45) and (44), we obtain:

$$C_n = \frac{B_n}{2m_2} \left[- \left((k_1 + k_2 - 2m_1\nu_{1n}) \cos(m_2\alpha x_{min}) + 2m_2 \sin(m_2\alpha x_{min}) \right) \cos(m_1\alpha x_{min}) \right. \\ \left. + \left(((k_1 + k_2)\nu_{1n} + 2m_1) \cos(m_2\alpha x_{min}) + 2m_2\nu_{1n} \sin(m_2\alpha x_{min}) \right) \sin(m_1\alpha x_{min}) \right], \quad (\text{A1})$$

$$D_n = \frac{B_n}{2m_2} \cos(m_2\alpha x_{min}) \left[\left(-2m_2\nu_{1n} + (2m_1 + (k_1 + k_2)\nu_{1n}) \tan(m_2\alpha x_{min}) \right) \sin(m_1\alpha x_{min}) \right. \\ \left. + \left(2m_2 - (k_1 + k_2 - 2m_1\nu_{1n}) \tan(m_2\alpha x_{min}) \right) \cos(m_1\alpha x_{min}) \right]. \quad (\text{A2})$$

Solving for C_n and D_n in terms of H_n using Eqs. (48) and (49), we obtain:

$$C_n = \frac{-8m_3^2 H_n}{m_2[k_2^2 - k_3^2 + 8m_3^2 + (k_3^2 - k_2^2) \cos(2m_3\beta x_{max})]} \times \left[\left[\frac{k_2}{2} \cos(m_3\beta x_{max}) - \left(m_3 + \frac{k_2(k_2 + k_3)}{4m_3} \right) \sin(m_3\beta x_{max}) \right] \left[\cos(m_4\beta x_{max}) - \nu_{4n} \sin(m_4\beta x_{max}) \right] - \left[\frac{1}{2} \cos(m_3\beta x_{max}) + \frac{k_2 + k_3}{4m_3} \sin(m_3\beta x_{max}) \right] \left[(k_4 - 2m_4\nu_{4n}) \cos(m_4\beta x_{max}) - (2m_4 + \nu_{4n}k_4) \sin(m_4\beta x_{max}) \right] \right], \quad (\text{A3})$$

$$D_n = \frac{4m_3 H_n}{k_2^2 - k_3^2 + 8m_3^2 + (k_3^2 - k_2^2) \cos(2m_3\beta x_{max})} \times \left[2m_3 \cos(m_3\beta x_{max}) \left[\cos(m_4\beta x_{max}) - \nu_{4n} \sin(m_4\beta x_{max}) \right] + \sin(m_3\beta x_{max}) \left[(2m_4 + (k_3 + k_4)\nu_{4n}) \sin(m_4\beta x_{max}) - (k_3 + k_4 - 2m_4\nu_{4n}) \cos(m_4\beta x_{max}) \right] \right]. \quad (\text{A4})$$

- ¹E. B. Mpemba and D. G. Osborne, “Cool?” *Phys. Educat.* **4**, 172–175 (1969).
- ²S. M. Mirabedin and F. Farhadi, “Numerical investigation of solidification of single droplets with and without evaporation mechanism,” *Int. J. Refrig.* **73**, 219 – 225 (2017).
- ³M. Vynnycky and S. Kimura, “Can natural convection alone explain the mpemba effect?” *Int. J. Heat Mass Transf.* **80**, 243 – 255 (2015).
- ⁴J. I. Katz, “When hot water freezes before cold,” *Am. J. Phys.* **77**, 27–29 (2009).
- ⁵D. Auerbach, “Supercooling and the mpemba effect: When hot water freezes quicker than cold,” *Am. J. Phys.* **63**, 882–885 (1995).
- ⁶X. Zhang, Y. Huang, Z. Ma, Y. Zhou, J. Zhou, W. Zheng, Q. Jiang, and C. Q. Sun, “Hydrogen-bond memory and water-skin supersolidity resolving the mpemba paradox,” *Phys. Chem. Chem. Phys.* **16**, 22995–23002 (2014).
- ⁷Y. Tao, W. Zou, J. Jia, W. Li, and D. Cremer, “Different ways of hydrogen bonding in water - why does warm water freeze faster than cold water?” *J. Chem. Theory Comput.* **13**, 55–76 (2017).
- ⁸J. Jin and W. A. Goddard III, “Mechanisms underlying the mpemba effect in from molecular dynamics simulations,” *J. Phys. Chem. C* **119**, 2622–2629 (2015).
- ⁹A. Gijón, A. Lasanta, and E. Hernández, “Paths towards equilibrium in molecular systems: The case of water,” *Phys. Rev. E* **100**, 032103 (2019).
- ¹⁰P. Chaddah, S. Dash, K. Kumar, and A. Banerjee, “Overtaking while approaching equilibrium,” arXiv preprint arXiv:1011.3598 (2010).
- ¹¹C. Hu, J. Li, S. Huang, H. Li, C. Luo, J. Chen, S. Jiang, and L. An, “Conformation directed mpemba effect on polylactide crystallization,” *Cryst. Growth Des.* **18**, 5757–5762 (2018).
- ¹²Y.-H. Ahn, H. Kang, D.-Y. Koh, and H. Lee, “Experimental verifications of mpemba-like behaviors of clathrate hydrates,” *Korean J. Chem. Eng.* **33**, 1903–1907 (2016).
- ¹³A. Kumar and J. Bechhoefer, “Exponentially faster cooling in a colloidal system,” *Nature* **584**, 64–68 (2020).
- ¹⁴A. Kumar, R. Chetrite, and J. Bechhoefer, “Anomalous heating in a colloidal system,” arXiv preprint arXiv:2104.12899 (2021).
- ¹⁵J. Bechhoefer, A. Kumar, and R. Chetrite, “A fresh understanding of the mpemba effect,” *Nature Reviews Physics*, 1–2 (2021).
- ¹⁶A. Gal and O. Raz, “Precooling strategy allows exponentially faster heating,” *Phys. Rev. Lett.* **124**, 060602 (2020).
- ¹⁷I. Klich, O. Raz, O. Hirschberg, and M. Vucelja, “Mpemba index and anomalous relaxation,” *Phys. Rev. X* **9**, 021060 (2019).
- ¹⁸I. Klich and M. Vucelja, “Solution of the metropolis dynamics on a complete graph with application to the markov chain mpemba effect,” arXiv preprint arXiv:1812.11962 (2018).
- ¹⁹S. K. Das and N. Vadakkayil, “Should a hotter paramagnet transform quicker to a ferromagnet? monte carlo simulation results for ising model,” *Phys. Chem. Chem. Phys.* (2021).
- ²⁰I. González-Adalid Pemartín, E. Mompó, A. Lasanta, V. Martín-Mayor, and J. Salas, “Slow growth of magnetic domains helps fast evolution routes for out-of-equilibrium dynamics,” *Phys. Rev. E* **104**, 044114 (2021).
- ²¹G. Teza, R. Yaacoby, and O. Raz, “Relaxation shortcuts through boundary coupling,” arXiv preprint arXiv:2112.10187 (2021).
- ²²M. Baity-Jesi, E. Calore, A. Cruz, L. A. Fernandez, J. M. Gil-Narvián, A. Gordillo-Guerrero, D. Iñiguez, A. Lasanta, A. Maiorano, E. Marinari, *et al.*, “The mpemba effect in spin glasses is a persistent memory effect,” *Proc. Natl. Acad. Sci. USA* **116**, 15350–15355 (2019).
- ²³A. Santos and A. Prados, “Mpemba effect in molecular gases under nonlinear drag,” *Phys. Fluids* **32**, 072010 (2020).
- ²⁴R. Gómez González, N. Khalil, and V. Garzó, “Mpemba-like effect in driven binary mixtures,” *Physics of Fluids* **33**, 053301 (2021).
- ²⁵R. G. González and V. Garzó, “Anomalous mpemba effect in binary molecular suspensions,” arXiv preprint arXiv:2011.13237 (2020).
- ²⁶A. Patrón, B. Sánchez-Rey, and A. Prados, “Strong nonexponential relaxation and memory effects in a fluid with nonlinear drag,” *Phys. Rev. E* **104**, 064127 (2021).
- ²⁷Z. Lu and O. Raz, “Nonequilibrium thermodynamics of the markovian mpemba effect and its inverse,” *Proc. Natl. Acad. Sci. USA* **114**, 5083–5088 (2017).
- ²⁸T. Van Vu and Y. Hasegawa, “Toward relaxation asymmetry: Heating is faster than cooling,” *Phys. Rev. Research* **3**, 043160 (2021).
- ²⁹M. R. Walker and M. Vucelja, “Anomalous thermal relaxation of langevin particles in a piecewise-constant potential,” *Journal of Statistical Mechanics: Theory and Experiment* **2021**, 113105 (2021).
- ³⁰D. M. Busiello, D. Gupta, and A. Maritan, “Inducing and optimizing markovian mpemba effect with stochastic reset,” *New Journal of Physics* **23**, 103012 (2021).
- ³¹A. Lapolla and A. Godec, “Faster uphill relaxation in thermodynamically equidistant temperature quenches,” *Physical Review Letters* **125**, 110602 (2020).
- ³²J. Degünther and U. Seifert, “Anomalous relaxation from a non-equilibrium steady state: An isothermal analog of the mpemba effect,” *Europhysics Letters* **139**, 41002 (2022).
- ³³M. R. Walker and M. Vucelja, “Mpemba effect in terms of mean first passage times of overdamped langevin dynamics on a double-well potential,” arXiv preprint arXiv:2212.07496 (2022).
- ³⁴F. J. Schwarzendahl and H. Löwen, “Anomalous cooling and

- overcooling of active colloids,” *Phys. Rev. Lett.* **129**, 138002 (2022).
- ³⁵F. Carollo, A. Lasanta, and I. Lesanovsky, “Exponentially accelerated approach to stationarity in markovian open quantum systems through the mpemba effect,” *Phys. Rev. Lett.* **127**, 060401 (2021).
- ³⁶A. Nava and M. Fabrizio, “Lindblad dissipative dynamics in the presence of phase coexistence,” *Physical Review B* **100**, 125102 (2019).
- ³⁷A. K. Chatterjee, S. Takada, and H. Hayakawa, “Quantum mpemba effect in a quantum dot with reservoirs,” arXiv preprint arXiv:2304.02411 (2023).
- ³⁸R. Holtzman and O. Raz, “Landau theory for the mpemba effect through phase transitions,” *Communications Physics* **5**, 280 (2022).
- ³⁹S. Zhang and J.-X. Hou, “Theoretical model for the mpemba effect through the canonical first-order phase transition,” *Physical Review E* **106**, 034131 (2022).
- ⁴⁰G. Teza, R. Yaacoby, and O. Raz, “Eigenvalue crossing as a phase transition in relaxation dynamics,” arXiv preprint arXiv:2209.09307 (2022).
- ⁴¹A. Lasanta, F. Vega Reyes, A. Prados, and A. Santos, “When the hotter cools more quickly: Mpemba effect in granular fluids,” *Phys. Rev. Lett.* **119**, 148001 (2017).
- ⁴²A. Torrente, M. A. López-Castaño, A. Lasanta, F. V. Reyes, A. Prados, and A. Santos, “Large mpemba-like effect in a gas of inelastic rough hard spheres,” *Phys. Rev. E* **99**, 060901 (2019).
- ⁴³E. Mompó, M. Castaño, A. Torrente, F. V. Reyes, and A. Lasanta, “Memory effects in a gas of viscoelastic particles,” arXiv preprint arXiv:2006.00241 (2020).
- ⁴⁴A. Biswas, V. V. Prasad, O. Raz, and R. Rajesh, “Mpemba effect in driven granular maxwell gases,” *Phys. Rev. E* **102**, 012906 (2020).
- ⁴⁵A. Biswas, V. V. Prasad, and R. Rajesh, “Mpemba effect in an anisotropically driven granular gas,” *EPL (Europhysics Letters)* (2021).
- ⁴⁶A. Biswas, V. Prasad, and R. Rajesh, “Mpemba effect in anisotropically driven inelastic maxwell gases,” *Journal of Statistical Physics* **186**, 1–21 (2022).
- ⁴⁷A. Megias and A. Santos, “Mpemba-like effect protocol for granular gases of inelastic and rough hard disks,” *Frontiers in Physics* , 739 (2022).
- ⁴⁸A. Biswas, V. V. Prasad, and R. Rajesh, “Mpemba effect in driven granular gases: role of distance measures,” arXiv preprint arXiv:2303.10900 (2023).
- ⁴⁹H. Risken, “Fokker-planck equation,” in *The Fokker-Planck Equation* (Springer, 1996) pp. 63–95.
- ⁵⁰C. W. Gardiner *et al.*, *Handbook of stochastic methods*, Vol. 3 (springer Berlin, 1985).
- ⁵¹M. Mörsch, H. Risken, and H. Vollmer, “One-dimensional diffusion in soluble model potentials,” *Zeitschrift für Physik B Condensed Matter* **32**, 245–252 (1979).